Received: 14 May 2021 | Revised: 12 July 2021 | Accepted: 9 August 2021

DOI: 10.1002/cey2.151

RESEARCH ARTICLE

CARBON ENERGY WILEY

Fibrous gel polymer electrolyte for an ultrastable and highly safe flexible lithium-ion battery in a wide temperature range

Ke Li | **Wei Shen** | **Tao Xu** | **Lu Yang** | **Xiaobing Xu** | **Feiyao Yang** | **Lijuan Zhang** | **Yangjian Wang** | **Yaning Zhou** | **Mengjuan Zhong** | **Di Wei**

Division of G-Device Technology, Beijing Graphene Institute, Beijing, China

Correspondence
Di Wei, Division of G-Device Technology, Beijing Graphene Institute, Beijing 100094, China.
Email: diwei@hotmail.com

Funding information
Beijing Municipal Science and Technology Commission, Grant/Award Numbers: Z181100001018029, Z181100004818004, Z191100006119027

Abstract

Replacement of flammable liquid electrolytes with gel polymer electrolytes (GPEs) is a promising route to improve the safety of lithium-ion batteries (LIBs). However, polymer-based electrolytes have limited suitability at low/high temperatures due to the instability of the polymer at high temperatures and the low ionic conductivity of the gel state at low temperatures. Herein, an integrated design of electrodes/fibrous GPEs modified with graphene oxide (GO) is reported. Due to the integrated structure of electrodes/GPEs, the strong interface affinity between electrodes and GPEs ensures that the GPEs spun on electrodes do not shrink at high temperatures (160–180°C), thus preventing a short circuit of electrodes. Moreover, after GO modification, oxygen-containing functional groups of GO can accelerate Li^+ transport of GO-GPEs even at a low temperature of −15°C. When these GPEs are applied to flexible LIBs, the LIBs show excellent electrochemical performance, with satisfactory cycling stability of 82.9% at 1 C after 1000 cycles at 25°C. More importantly, at a high temperature of 160°C, the LIBs can also discharge normally and light the green light-emitting diode. Furthermore, at a low temperature of −15°C, 92.7% of its room-temperature capacity can be obtained due to the accelerated Li^+ transport caused by GO modification, demonstrating the great potential of this electrolyte and integrated structure for practical gel polymer LIB applications.

KEYWORDS
flexible battery, gel polymer electrolyte, graphene oxide, safe lithium-ion battery

1 | INTRODUCTION

Flexible electronics have received considerable attention in recent years. These devices are part of our daily lives and are of interest in the development of futuristic electronics.[1,2] Flexible electronics should be flexible, bendable, or naturally foldable for integration with the human body to develop the ubiquitous applications that are considered as the next-generation revolution.[3–5] The technology trends of flexible electronics may advance

from the curved screen to the foldable screen and eventually to the flexible screen. The Samsung Galaxy S7 Edge provides an excellent grip thanks to its curved screen.[6] Moreover, Apple recently sent the iPhone with a foldable screen to Foxconn for testing, requiring it to be folded more than 100,000 times.[7] Therefore, flexible batteries, especially LIBs for energy storage, should also be developed to fulfill the power requirements of flexible electronics. To meet the needs for flexible electronics, successful development of flexible, inexpensive, long-life, safe, lightweight, and environmentally friendly flexible LIBs is a key prerequisite.[8–10] Previously, we have successfully developed flexible LIBs based on carbon nanotube paper and graphene paper, which can be bent more than 100,000 times.[11,12] However, these improvements are mainly focused on the current collector, mainly improving the flexibility of the battery. The potential safety problems of LIBs in a wide range of temperatures still exist. This paper proposes a new technology to improve the safety of flexible LIBs.

Conventional LIBs are composed of several main components including a cathode, an anode, a separator, an electrolyte, a current collector, and package materials.[13,14] Polyolefin-based separators, such as Celgard, and a liquid electrolyte are usually used in conventional LIBs, which can easily lead to electrolyte leakage and short circuit of the battery, consequently leading to huge safety hazards. Some catastrophic accidents have happened owing to the use of a liquid electrolyte and polyolefin-based separators, such as spontaneous combustion of Samsung Note7.[15] In flexible LIBs, the battery is required to be capable of deformation, so it is more likely to cause damage to the packaging material, electrolyte leakage, and battery safety accidents. Therefore, improving safety is particularly important for flexible LIBs.

GPEs are attracting increasing interest and are regarded as promising candidates to solve the potential safety issues of LIBs.[16] Compared with liquid electrolytes, GPEs have several advantages as membranes in terms of no internal shorting, no leakage of liquid electrolytes, and nonflammability.[17,18] Moreover, GPEs also have good flexibility and high ionic conductivity, which are suitable for practical applications in flexible LIBs.[19] However, the current LIBs using GPEs usually adopt the three-layer superposition preparation technology of a cathode, an anode, and GPEs. In particular, the interface affinity between GPEs and electrodes is poor during battery bending, which results in the large internal resistance of the battery system and degradation of electrochemical performance.[20–23] In addition, GPEs composed of polymers still shrink at higher temperatures and the safety is significantly lower than that of all-solid-state inorganic electrolytes. Therefore, there is an urgent need for further improving the thermal stability and electrochemical performance of GPEs to realize their practical application in flexible LIBs.

In this study, we present a safety-reinforced and high-performance flexible LIB based on the integrated design of electrodes/fibrous GPEs (graphene oxide [GO]-modified poly (vinylidene fluoride-tri-fluoroethylene-chlorofluoroethylene) [PTC]). As a new type of material, PTC has so far barely been reported in the field of LIBs. The highest dielectric constant of PTC (50–57), compared to previously reported PE (polyethylene) (2.3), PP (polypropylene) (2.2–2.3), PEO (poly(ethylene oxide)) (~5), PAN (polyacrylonitrile) (5.5), PMMA (poly(methyl methacrylate)) (3.0), and polyvinylidene difluoride (PVDF) (8.15–10.46), is critical to GPEs through improving the dissociation degree of $LiPF_6$.[24] Increasing the dissociation degree of $LiPF_6$ can lead to a further increase in the ionic conductivity of GPE, thus improving the electrochemical performance. Moreover, polymer-based gel electrolytes are usually difficult to use at low temperatures due to the low ionic conductivity of the gel state at low temperatures.[25–28] In this study, after GO modification, oxygen-containing functional groups of GO could accelerate Li^+ transport, thereby enabling their application at a low temperature of −15°C, with 92.7% of its room-temperature capacity. In addition, as GPEs are spun directly to the surface of electrodes, the interface affinity between the electrodes and the GPEs is significantly improved. As a result, excellent cyclic stability is obtained for the flexible full battery ($LiCoO_2$ as a cathode, denoted LCO, graphite as an anode) even during the bending of the battery. More importantly, due to the strong affinity between GPEs and electrodes, the LIBs can also discharge normally and light the green light-emitting diode (LED) at a high temperature of 160°C. Even at a higher temperature of 180°C, GPEs still do not shrink but will show a closed-hole reaction, so that flexible LIBs will automatically cut off the working state at a high temperature without a short circuit. Therefore, flexible LIBs using GPEs have the characteristics of high-temperature resistance, nonflammability, and protection from explosion.

2 | EXPERIMENTAL SECTION

2.1 | Materials

PTC (MW ≈ 400,000–600,000) was purchased from Wuhan Methyl Technology Co., Ltd. GO (sheet diameter of 30–50 μm, thickness of 1.0–1.77 nm, number of layers 1–5) powder was purchased from Suzhou Tanfeng Graphene Technology Co., Ltd. Anhydrous ethanol, *N*, *N*-dimethylformamide (DMF), and acetonitrile were purchased from Sinopharm Chemical Reagent Co., Ltd. The 1.0 M $LiPF_6$-ethylene carbonate (EC)/diethyl

carbonate (DEC) (1:1, volume/volume) with 5.0% FEC (fluoroethylene carbonate) was purchased from Suzhou Duoduo Chemical Technology Co., Ltd.

2.2 | Fabrication of electrodes and GPE

The schematic diagram of the integrated design process of electrodes/fibrous GPEs for preparing gel polymer flexible LIBs is shown in Figure S1. The preparation of electrodes and GPEs mainly includes the following steps through a small production line: (1) A uniformly mixed slurry of the LCO cathode and the graphite anode was separately prepared using a vacuum planetary mixing device. (2) To prepare the electrodes, the LCO and graphite slurry were separately scraped onto the surface of an Al foil and a Cu foil using an automatic scraper coater. Then, they were dried at 100°C in a vacuum for at least 10 h. (3) The electrodes of LCO and graphite were rolled to increase the compaction density using a double-roll machine. (4) GO-modified fibrous PTC-based gel polymer electrolyte (GO-GPE) nanofiber membranes on the electrode surface were prepared using an electrospinning method. (5) An LCO cathode and a graphite anode stacked face to face were rolled and compounded into a whole. (6) The integrated electrodes of LCO and graphite with the obtained fiber-based porous membranes were then dried in vacuum at 75°C for 48 h, which was to ensure that the organic solvent was completely removed. (7) The dried integrated electrodes of LCO and graphite were cut into the required size and assembled into flexible LIBs. LCO (Shenzhen Kejing Star Technology Ltd.) was used as a cathode. Graphite (Shenzhen Kejing Star Technology Ltd.) was used as an anode. The cathode is composed of LCO, super P as a conductive additive, and PVDF as a binder (95:2.5:2.5 weight ratio). The anode is composed of graphite, super P, styrene–butadiene rubber as a binder, and carboxyl methylcellulose as a thickener (94.5:1:2.25:2.25 weight ratio). The LCO slurry was spread onto an Al foil. The graphite slurry was spread onto a Cu foil. Pristine fibrous PTC-based GPE (P-GPE) and GO-GPE nanofiber membranes on the electrode surface were prepared using an electrospinning method. To prepare GO-GPE nanofiber membranes, GO (0.03 g) was dispersed in DMF (12 g) using a sonicator for 90 min, and PTC (2.97 g) was then added and mixed using a planetary mixer for 30 min to obtain a homogeneous slurry. Next, the resulting homogeneous slurry was filled and stored in a 10 ml syringe. Then, the GO-GPE fibrous membrane was fabricated by electrospinning with positive voltage (15 kV) and negative voltage (2 kV) at room temperature, and the syringe pump feeding rate was 1.0 ml/h. The distance between the steel needle tip of the syringe and the rotating drum collector was 30 cm, and the speed of drum spin was 50 rpm. For comparison, a controlled P-GPE sample was also prepared, and the synthetic process was the same as mentioned above, except for the addition of GO. The cathode and anode located in the rotating drum were used to collect the resulting fibers. The obtained fiber-based porous membranes on the cathode and the anode were then dried in a vacuum at 75°C for 48 h. Finally, the obtained sample was swollen in a liquid electrolyte (1.0 M $LiPF_6$ in EC/DEC = 1:1, volume/volume with 5.0% FEC) for 1 h, ultimately yielding P-GPE and GO-GPE.

2.3 | Electrochemical test for coin cells

Coin half-cells (2032) were assembled in an Ar-filled glovebox using an Li foil as the counter electrode. The cathode and anode materials loaded in each coin cell were typically 12–13 and 5–6 mg cm^{-2}, respectively. A commercial polypropylene microporous film (Celgard 2300), P-GPE, and GO-GPE as the separator were used. The assembled coin cells were cycled at different charge/discharge rates on a Land battery tester (Wuhan Land Electronic Co. Ltd.).

2.4 | Electrochemical test for a flexible battery

A flexible lithium-ion battery (full cell) was assembled with LCO as a cathode and graphite as an anode. Each electrode had the same composition as the corresponding coin cell electrode. GO-GPE was chosen as the separator. The N/P ratio (negative electrode capacity/positive electrode capacity) was 1.05. The assembled full cells were cycled at different charge/discharge rates at −15°C, 25°C, 45°C, 60°C, and 80°C on a Land battery tester (Wuhan Land Electronic Co. Ltd.). Galvanostatic charge/discharge was carried out in a voltage window of 3.0–4.35 V.

2.5 | Electrochemical evaluation

The ionic conductivity (σ) of the commercial Celgard separator and GPEs was characterized using the alternating current impedance method (Metrohm; Autolab) with the potential amplitude of 5 mV using the first applied frequency of 10^6 Hz and the last applied frequency of 0.1 Hz by assembling a coin cell with a symmetrical structure SS | GPE | SS (SS, stainless steel). The ionic conductivity (σ, S cm^{-1}) of the commercial Celgard

separator and GPE was calculated according to the following equation[55]:

$$\sigma = \frac{d}{SR_b}.$$

The vertical distance from one electrode to the other is d (cm), S is the effective area of the commercial Celgard separator and GPEs (cm^2), and the bulk resistance of the Celgard separator and GPEs is R_b (Ω). Coin cells were used to test the lithium-ion migration number (t_+) of the Celgard separator and GPEs at room temperature with Li | GPE | Li (Li, lithium metal foil) structures according to the following equation[56]:

$$t_+ = \frac{I_s(\Delta V - I_0 R_0)}{I_0(\Delta V - I_s R_s)},$$

where ΔV is the selected polarization voltage (mV); I_0 is the initial current (mA), I_s is the steady-state current, R_0 is the initial resistance (Ω), and R_s is the steady-state resistance. The coin cell of Li/PSPE/Li was used to test cell polarization by charge and discharge tests with a constant current of 10 mV s^{-1}.

2.6 | Characterization methods

The morphology and microstructure of the samples were examined using field-emission scanning electron microscopy (FE-SEM; Supra 55; Zeiss). The open-circuit voltage (OCV) analysis was carried out using the Autolab (Metrohm). The specific surface area of the GPE was determined from N_2 adsorption isotherms (MicrotracBEL; BELSORP-max). The bending test was performed using a specially designed stepper motor. Thermal stability analysis was performed using a DSC-TGA (STA 449 F5; NETZSCH). The pore diameter and the pore diameter distribution were determined using a comprehensive membrane pore size analyzer (BSD-PB; Beishide). The vibrational changes of samples were determined by Fourier-transform infrared spectra (FTIR; IRTracer-100; Shimadzu) in the wavenumber range from 500 to 4000 cm^{-1} in attenuated total reflection.

3 | RESULTS AND DISCUSSION

3.1 | Properties of PTC-based GPE

The integrated design process of electrodes/fibrous GPEs is shown in Figure S1. The surface morphology of P-GPE and GO-GPE was clearly determined by FE-SEM. As shown in Figure S2a–c, FE-SEM images revealed that the P-GPE membrane has an uneven fibrous diameter, a relatively smooth surface, and some bead structures in the white circles, which is detrimental to the electrochemical performance of LIBs. In comparison, the GO-GPE membrane had a more evenly fibrous diameter (-Figure S2e–g) and a rougher surface without any bead structures compared to the control P-GPE membrane, thanks to the suitable viscosity of the electrospinning slurry by the addition of GO. The addition of GO led to an increase in viscosity and change in surface tension and an alteration in the electrostatic repulsion of the slurry, thus improving the surface morphology of the membrane.[29,30] Furthermore, the fibrous membranes have a smaller thickness (~15 μm) as compared to the commercial Celgard separator (~25 μm) and excellent interface compatibility with LCO cathodes.[31] As shown in Figure S2d,h, the cross-section images of the LCO cathode with P-GPE and GO-GPE membranes indicated that the membranes were in close contact with the LCO cathode, which contributes toward reducing the interface resistance between the electrode and GPEs.

The melting temperatures of the separator and GPEs are a vital physical parameter for the operating temperature and the thermal runaway of LIBs. Therefore, differential scanning calorimetry (DSC) analysis was performed, and the melt curves are shown in Figure S3. The melting temperatures of PTC-based fibrous membranes are close to those of the Celgard separator at ~167°C. However, an additional endothermic peak in the Celgard separator appears at ~135°C due to the preparation method of the Celgard separator with uniaxial stretching,[32] which is disadvantageous for the safety of LIBs. The endothermic peak temperature of the Celgard separator at 135°C is far less than its melting temperature of 167°C, possibly resulting in thermal shrinkage when the temperature is higher than 135°C. This will further lead to short circuits and thermal runaway of the corresponding LIBs. To verify the above results, the thermal shrinkage of the Celgard separator and various GPE membranes was evaluated. The surface morphology of the Celgard separator, P-GPE, and GO-GPE before and after thermal treatment at 160°C for 1 h is shown in Figure 1, and the corresponding overall size change is shown in the insets of Figure 1. After the thermal treatment, shrinkage of the Celgard separator to half its size could be easily observed, as shown in the insets of Figure 1A,B, and the porous structure had completely disappeared. As a comparison, the integral sizes of P-GPE and GO-GPE still remained unchanged after the thermal treatment at 160°C (insets of Figure 1C–F). In addition, the FE-SEM analysis revealed that the fiber diameter and the network structure of PTC-based fibrous membranes

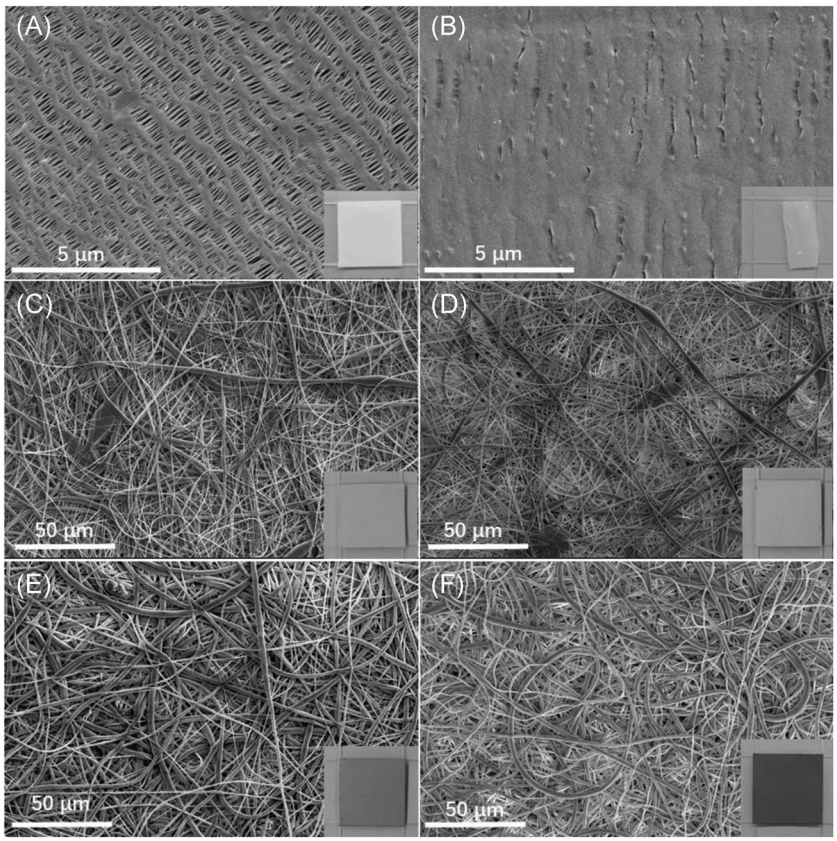

FIGURE 1 FE-SEM images of (A,B) a commercial Celgard separator, (C,D) P-GPE, and (E, F) GO-GPE. (A,C,E) Before and (B,D,F) after thermal treatment at 160°C for 1 h (Inset: Corresponding photographs). GO, graphene oxide; GO-GPE, GO-modified fibrous PTC-based gel polymer electrolyte; P-GPE, pristine fibrous PTC-based GPE; PTC, poly(vinylidene fluoride-tri-fluoroethylene-chlorofluoroethylene); FE-SEM, field-emission scanning electron microscopy

showed almost no significant change after treatment at 160°C (Figure 1).

When the thermal treatment temperature was further increased to 180°C for 1 h, the bare GO-GPE membrane without the LCO cathode shrank considerably (Figure 2A), and this was in good agreement with the DSC results (Figure S3). However, the GO-GPE spun onto the LCO cathode, named GO-GPE/LCO, barely shrank inside (Figure 2C) and on the edges (Figure 2D–F). The only difference from before thermal treatment was that the GO-GPE membrane had melted and obturated, resulting in a decrease in the thickness of the GO-GPE membrane from ~15 to ~8 μm. Compared with GO-GPE, the thermal stability of P-GPE (Figure S4) decreased slightly at 180°C, but the Celgard separator (Figure S5) showed poor thermal stability at 180°C, as shown in Figures S4 and S5. In Figures 2A and S4a, the bare P-GPE membrane showed more severe shrinkage than the bare GO-GPE membrane when the thermal treatment temperature was further increased to 180°C. Meanwhile, the Celgard separator completely melted after heating at 180°C for 1 h (Figure S5a). However, the P-GPE spun onto the LCO cathode, named P-GPE/LCO, barely shrank within (Figure S4c), but the P-GPE/LCO showed slight shrinkage on the edges (Figure S4d–f). Moreover, this shrinkage stress caused a huge gap between the LCO cathode and the Al foil (Figure S4e,f), which led to a marked decrease in the electrochemical performance of LIBs. More importantly, the shrinkage occurred on the edges of P-GPE/LCO, which may pose safety issues, such as short circuits and thermal runaway of LIBs. The improved thermal stability of GO-GPE/LCO compared to P-GPE/LCO may be due to the continuous three-dimensional skeleton structure formed by GO in GO-GPE. By contrast, the Celgard separator stacked on top of the LCO cathode, named Celgard separator/LCO, showed marked shrinkage both within (Figure S5b,c) and on the edges (Figure S5b,d), which will inevitably lead to short circuit and thermal runaway of LIBs. In short, the excellent thermal stability of GO-GPE/LCO contributed toward improving the safety of LIBs at high temperatures, which can be explained in detail in combination with Figure 3.

Figure 3 shows the schematic diagram of conventional and gel polymer LIBs working at room temperature (25°C) and a high temperature (180°C), respectively. Both conventional and gel polymer LIBs work well at 25°C. When the ambient temperature increases to 180°C, the Celgard separator (PE or PP) will show considerable shrinkage, resulting in a short circuit of electrodes, which can increase local temperatures, ultimately resulting in the so-called thermal runaway of LIBs accompanied by smoke, flames, and explosion. However, GO-GPE/LCO barely shrank but melted and obturated. This contributes to ensuring that the battery does not short circuit. Moreover,

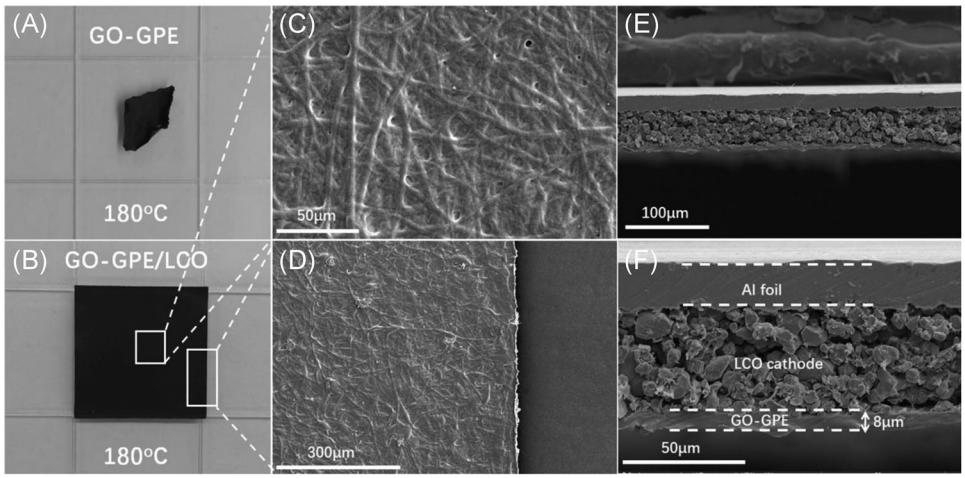

FIGURE 2 Optical photographs of the as-prepared (A) GO-GPE membrane and (B) the GO-GPE/LCO cathode after thermal treatment at 180°C for 1 h. FE-SEM images (C) within and (D) the edges of GO-GPE/LCO and (E, F) the cross-section images of the GO-GPE/LCO cathode. GO, graphene oxide; GO-GPE, GO-modified fibrous PTC-based gel polymer electrolyte; LCO, $LiCoO_2$; PTC, poly(vinylidene fluoride-tri-fluoroethylene-chlorofluoroethylene); FE-SEM, field-emission scanning electron microscopy

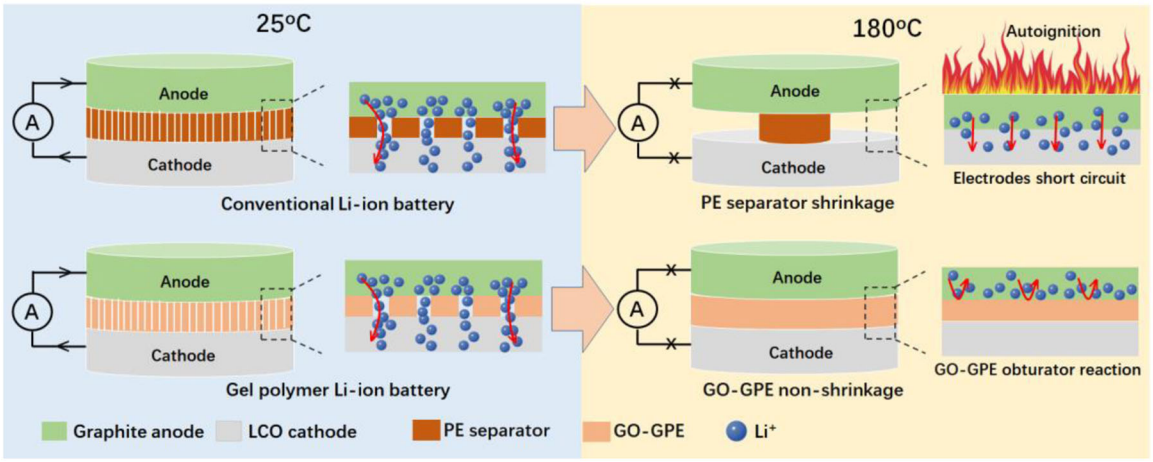

FIGURE 3 Schematic diagram of conventional and gel polymer lithium-ion batteries working at 25°C and 180°C, respectively. GO, graphene oxide; GO-GPE, GO-modified fibrous PTC-based gel polymer electrolyte; LCO, $LiCoO_2$; PE, polymer electrolyte; PTC, poly (vinylidene fluoride-tri-fluoroethylene-chlorofluoroethylene)

the melting and obturation of GO-GPE/LCO can further cut off the charging or discharging of LIBs, thus ensuring that thermal runaway of LIBs does not occur.

To further demonstrate the safety of the LIBs using fibrous GO-GPE, coin-type full cells connected in series with a green LED were tested at 25°C, 160°C, and 180°C. Before the test, coin-type full cells (LCO as the cathode, graphite as the anode) using a Celgard separator and GO-GPE were charged to the charging state and then exposed to 25°C, 160°C, and 180°C for 1 h. All coin cells can work well at 25°C (Figure 4A,D). However, when the temperature is increased to 160°C and 180°C, the thermal shrinkage of the Celgard separator can result in a direct short circuit between the cathode and the anode, ultimately resulting in voltage close to 0 V (Figure 4B,C). In contrast, due to the excellent thermal stability of fibrous GO-GPE membranes and the nonflammability of GO,[33,56] short circuit did not occur even at temperatures as high as 160°C and 180°C, and the voltage was still stable at ~3.0 V. However, it must be pointed out that the coin-type full cells could light the LED when the temperature reached 160°C, but they could not light the LED when the temperature reached 180°C due to the obturator of GO-GPE. This further demonstrates that fibrous GO-GPE will automatically cut off the charge and discharge of LIBs at high temperatures exceeding 180°C, thus preventing the occurrence of thermal runaway. Therefore, LIBs using GO-GPE have the characteristics of

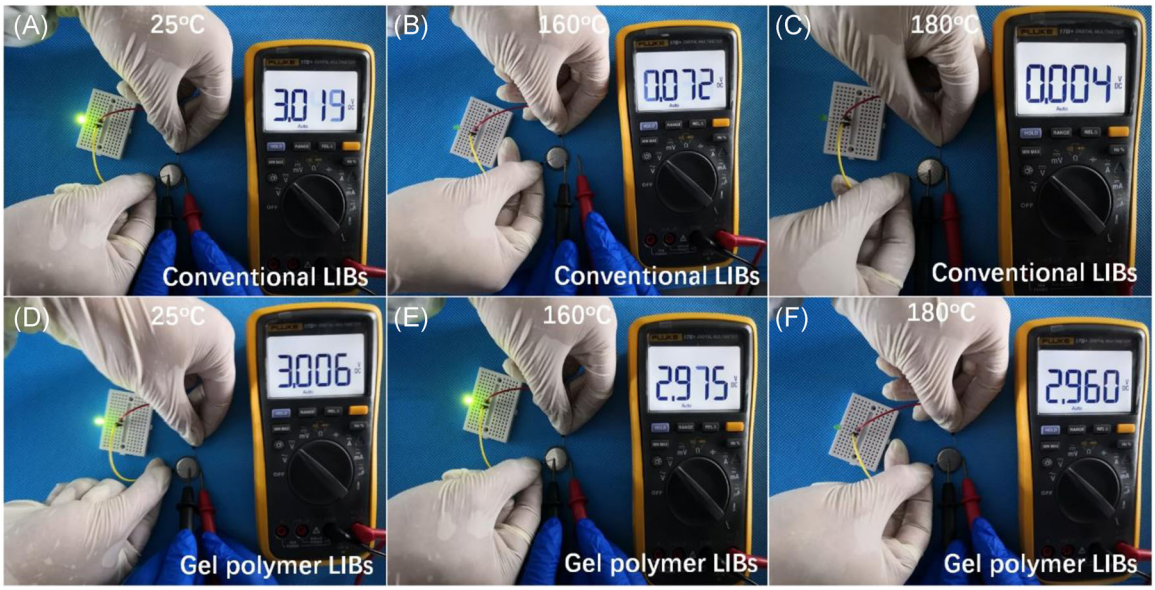

FIGURE 4 Optical images of (A–C) the conventional and (D–F) gel polymer coin-type full cells, connected to a voltmeter and a green light-emitting diode (LED). Coin-type full cells (A,D) before and after thermal treatment at (B,E) 160°C and (C,F) 180°C for 1 h. LIB, lithium-ion battery

high-temperature resistance, nonflammability, and protection against explosion. In addition, for conventional LIBs, lithium dendrites are usually easily produced on the anode in the long-term cycle process, thus resulting in the puncture of the separators further resulting in short circuits and thermal runaway. However, in our gel polymer LIBs, due to the excellent thermal stability of the fibrous GO-GPE, the local heat generated by a short circuit caused by lithium dendrites will lead to melting and obturation of the GO-GPE instead of shrinkage, thus ensuring that thermal runaway of LIBs does not occur to avoid explosion.

Moreover, the pore diameter distribution, porosity, and specific surface area are important physical parameters for GPEs and directly influence the electrochemical performance of LIBs. As shown in Figure S6, the distribution pores of GO-GPE were narrower (3.71–3.85 μm) than that of P-GPE within 4.65–5.68 μm. In addition, the porosity and specific surface area of P-GPE were 61.39% and 6.75 $m^2 g^{-1}$, respectively. However, with the addition of GO, the porosity and specific surface area of GO-GPE achieved higher values of 86.86% and 8.01 $m^2 g^{-1}$. This may be due to the markedly improved surface morphology of GO-GPE compared to P-GPE, such as a more evenly fibrous diameter and a rougher surface, and none revealed any bead structures.[34]

Moreover, the electrolyte uptake rate, electrolyte retention rate, ionic conductivity, and the lithium-ion transference number (t_{Li}^+) are also considered as key factors of GPEs, which are closely related to the pore diameter distribution, porosity, and specific surface area. The parameters of electrolyte uptake rate, electrolyte retention rate, ionic conductivity, and t_{Li}^+ of various membranes were measured, as shown in Figure 5. Compared with the P-GPE (1143.33%), the GO-GPE showed a much higher electrolyte uptake of 1541.43% and achieved better electrolyte retention of 60% (Figure 5A), which results from the much higher porosity and specific surface area. As confirmed through SEM observations, the uniform fiber of GO-GPE also leads to much higher porosity.[35–37] In addition, the GO-GPE had higher ionic conductivity than P-GPE and the Celgard separator from −20°C to 120°C (Figure 5B) and also showed higher t_{Li}^+ (0.83) than P-GPE (0.81) and the Celgard separator (0.28) at room temperature (Figure 5C).[38]

3.2 | Improvement mechanism of GO in GPEs

From the above results, it is clear that GO-GPE achieved the highest ionic conductivity and t_{Li}^+ among various samples, which may be a result of the existence of two types of lithium-ion transmission paths in GO-GPE (Figure 6). As shown in Figure 6A,B, the first path is the slow transport pathway in the pore, where the lithium-ion transport rate is the same as that in the bulk electrolyte. The second path is the fast transport pathway on the surface of GO-GPE fibers, where the lithium-ion transport rate is promoted by the –F groups of PTC and

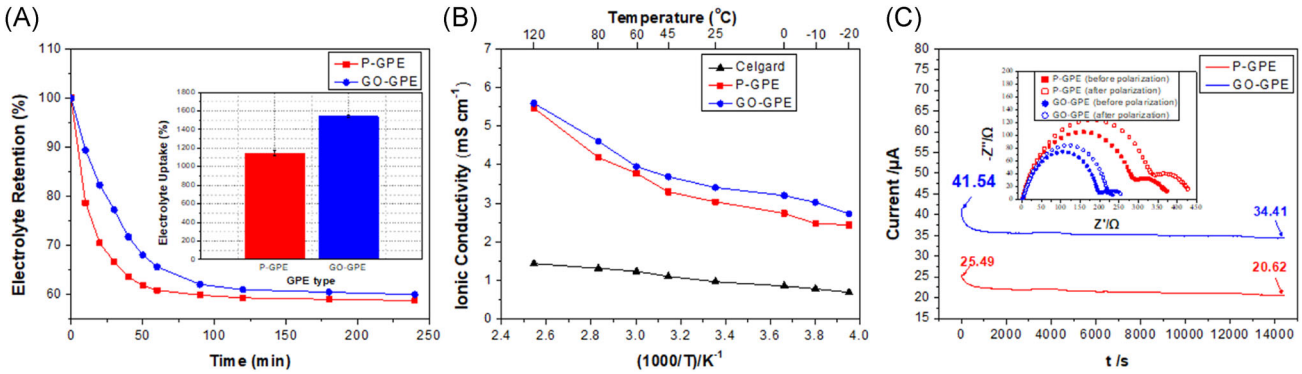

FIGURE 5 (A) Electrolyte retention of P-GPE and GO-GPE (Inset: Electrolyte uptake). (B) Ion conductivity of the Celgard separator and various GPEs at −20 to ~120°C. (C) Chronoamperometry profiles of Li | P-GPE | Li and Li | GO-GPE | Li cells at 25°C; the inset shows the electrochemical impendence spectrum at 25°C. GO, graphene oxide; GO-GPE, GO-modified fibrous PTC-based gel polymer electrolyte; P-GPE, pristine fibrous PTC-based GPE; PTC, poly(vinylidene fluoride-tri-fluoroethylene-chlorofluoroethylene)

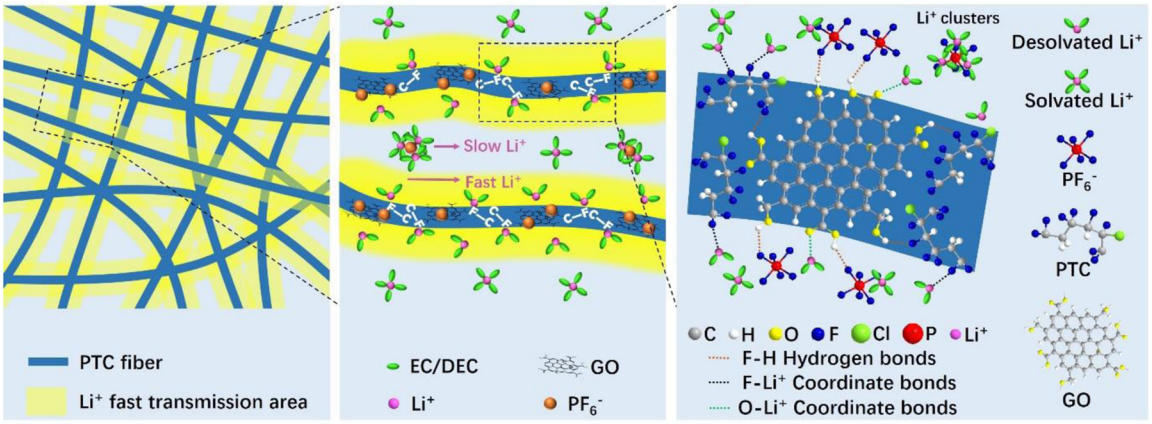

FIGURE 6 Schematic of the synergistic effect of the intermolecular hydrogen bond and the coordination bond in GO-GPE. DEC, diethyl carbonate; EC, ethylene carbonate; GO, graphene oxide; GO-GPE, GO-modified fibrous PTC-based gel polymer electrolyte; PTC, poly (vinylidene fluoride-tri-fluoroethylene-chlorofluoroethylene)

–COOH groups of GO. The reasons why the PTC-based gel electrolyte has higher ionic conductivity and t_{Li}^+ may be that (Figure 6C) (1) compared with the polyethylene of the Celgard separator (2.26–2.4),[39] PTC has a higher dielectric constant (50–57).[24] This can effectively promote the dissociation of $LiPF_6$ and desolvation of Li^+ with strong solvation,[40] thereby generating a large number of charge carriers and improving the ionic conductivity. (2) Fluorine with strong electronegativity was present in PTC, which can form an F–Li^+ coordination bond with Li^+ ions. Therefore, it can also effectively promote the dissociation of $LiPF_6$ and desolvation of Li^+ ions, thereby improving the ionic conductivity and t_{Li}^+.[40] Moreover, with the addition of GO, further improvement of ionic conductivity and t_{Li}^+ may probably be due to the following factors (Figure 6C): (1) The Li^+ ions can only be transported in the amorphous region of GPEs but not in the crystallization zone.[41] The fluorine in PTC can form H–F hydrogen bonds with the hydrogen of GO. The intermolecular hydrogen-bonding effect between PTC and GO may enable polymer chains to be more disordered in the copolymer, which promotes the formation of an amorphous region, yielding relatively low crystallinity.[42] The FTIR characterization of the GO-GPE fibrous membrane (Figure S7) confirmed the presence of H–F hydrogen bonds in the composites. All characteristic absorption peaks between 400 and 1500 cm^{-1} can be ascribed to PTC, which is consistent with previous work.[43] The absorption peaks of 1400 cm^{-1} (–CH_2– bending vibration), 1172 cm^{-1} (stretching band of C–F), and 873 cm^{-1} (band of the amorphous phase) are considered to be the characteristic absorption peaks of PTC. Compared to the P-GPE fibrous membrane, the C–F stretching band of the GO-GPE fibrous membrane was found to shift to 1171 from 1172 cm^{-1}, which confirms the presence of H–F hydrogen bonds.[44] (2) It can be

inferred from Figure S7 that the fluorine in PF_6^- ions may also form F–H hydrogen bonds with the hydrogen of –COOH and –OH on GO. As a result, the PF_6^- ions were highly attracted by GO-modified PTC chains, resulting in the formation of percolated space-charge pathways that significantly decrease the PF_6^- transport rate and promote the transport of Li^+ ions in GO-GPE.[45,46] Because of the synergistic effect of the above factors, the ion conductivity and t_{Li}^+ of GO-GPE increased markedly. (3) The electrostatic interaction between the oxygen-containing functional groups with unshared electron pairs on GO and Li^+ is assumed to facilitate desolvation of Li^+.[46]

3.3 | Electrochemical performance of coin cells and flexible full batteries

The electrochemical performances of as-fabricated LCO half-cells using a Celgard separator, P-GPE, and GO-GPE in the voltage window of 3.0–4.3 V (vs. Li/Li^+) are shown in Figure S8. In this study, 1 C = 163.3 mA g^{-1} for the LCO electrode. At room temperature, GO-GPE shows the best rate performance among various membranes, followed by P-GPE and the Celgard separator. It is very interesting that the variation trend of the electrochemical performance of various membranes shows consistency with the variation of the ionic conductivity, electrolyte uptake, and t_{Li}^+ (Figure S8a). Figure S8b shows the typical initial charge/discharge profiles of various membranes at 0.5 C. All membranes have similar voltage profiles and voltage platforms. In addition, the cycle performance of various membranes was investigated at 0.5 C, as shown in Figure S8c. Apparently, the cycle performances of half-cells using P-GPEs are in good agreement with the results obtained using the Celgard separator.

After studying the performance of the half-cells, the electrochemical study of the pouch-type flexible full cell was also performed in the voltage window of 3.0–4.35 V at different temperatures. The flexible full cell was assembled using LCO as a cathode, graphite as an anode, and fibrous GO-GPE membranes. Figure 7A shows the charge/discharge curves of the full cell at 25°C and at different current rates of 0.2, 0.5, 1, and 2 C. With an increase in the current rate, the charge/discharge voltage platform slowly increases/decreases, indicating a slight polarization caused by the high ionic conductivity of the GO-GPE. Accordingly, the GO-GPE shows excellent rate performance with good capacity retention of 161.3, 153.7, 141.8, and 122.2 mAh g^{-1} at 0.2, 0.5, 1, and 2 C, respectively, which also yields good capacity reversibility with a decrease in the current rate (Figure 7B). The long cycling stability of the full cell with GO-GPE at 25°C was tested by galvanostatic charge/discharge measurements at 1 and 2 C (Figure 7C). It is apparent that the full cell shows a stable long lifetime at various current densities. The initial discharge capacities of 135.4 and 119.9 mAh g^{-1} were obtained at 1 and 2 C, respectively. After 1000 cycles, the discharge capacities were 112.4 and 93.0 mAh g^{-1}, and the corresponding capacity retentions were approximately 82.9% and 77.5%, respectively. As shown in Figures 7C and S9, the cycling stability of the full cell with GO-GPE was relatively close to that of the full cell with a Celgard separator and a liquid electrolyte at 25 in 1 C, with the initial discharge capacity of 135.6 mAh g^{-1}. The long cycle life of the full cell with GO-GPE can fulfill the power requirements of flexible wearable and flexible digital products. Furthermore, as shown in Figure 7D–F, the electrochemical performance was also tested at a wide range of temperatures (−15°C to 80°C), and the corresponding capacities were 126.0, 135.9, 151.1, 148.6, and 151.3 mAh g^{-1} for −15°C, 25°C, 45°C, 60°C, and 80°C, respectively. Obviously, 92.7% of the room-temperature capacity remained at −15°C. The excellent low-temperature performance of GO-GPE ensures that the flexible battery can be used in a lower-temperature environment. Furthermore, to further explore the electrochemical performance of GO-GPE at higher temperatures, the GO-GPE was heated at 160°C and 180°C for 5 h. Then, it was assembled into a pouch-type flexible full cell. Subsequently, the cycling stability of the full cells with GO-GPE heated at different temperatures was tested at 25°C in 1 C (Figure S10). It is clear that the full cell with GO-GPE heated at 160°C shows initial discharge capacities of 140.4 and 82.0 mAh g^{-1} at the 20th cycle (Figure S10a,b). However, the full cell with GO-GPE heated at 180°C cannot work normally, which is due to the obturator of GO-GPE. In addition, almost uniform charge/discharge curves of the full cell with GO-GPE at 45°C, 60°C, 80°C, and 160°C were obtained, as shown in Figures 7F and S10b, indicating the excellent thermal stability of GO-GPE. Therefore, the excellent electrochemical performance in a wide range of temperatures helps to promote the practical application of GO-GPE and improve the safety of the LIBs using GO-GPE. Moreover, the change in OCV of the full cell at the charge state was tested under in situ bending conditions at a speed of 200 mm s^{-1} with a bending radius of 1 cm (Figure 7G). On using fibrous GO-GPE membranes, the voltage of the full cell barely decreased under in situ 1000 times mechanical bending. Furthermore, the flexibility of the full cell was further evaluated, as shown in Figure S11. After every 1000 times mechanical bending, a discharge specific capacity at 1 C was tested. Figure S11 shows the discharge-specific capacity of the full cell after different bending numbers. The cycle performance of full cell using GO-GPE is obviously better than that of Celgard

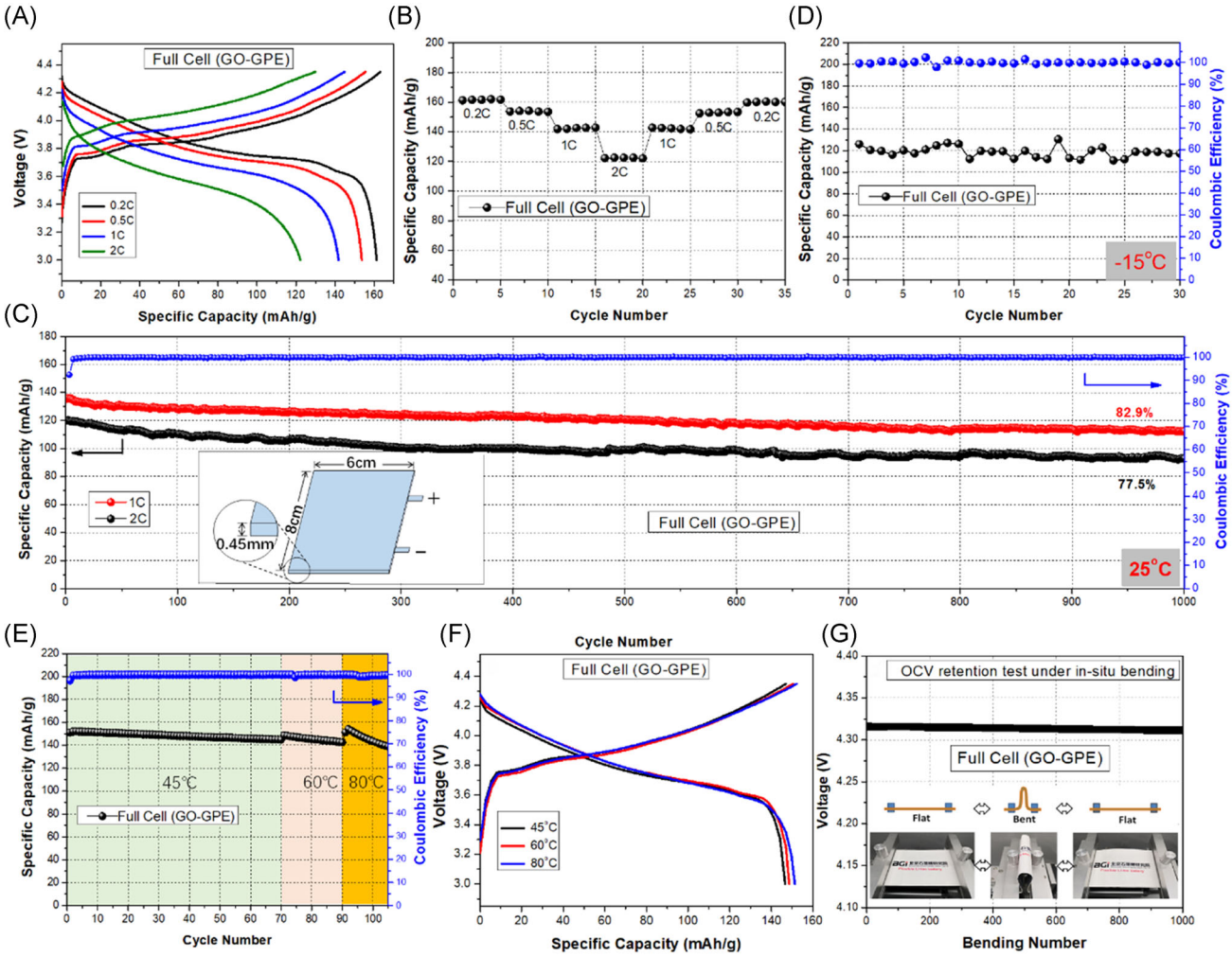

FIGURE 7 Electrochemical performances of a flexible LCO/graphite full battery using GO-GPE: (A) charge/discharge curves and (B) discharge capacities at various C-rates, (C) cycle performances at 25°C, (D) −15°C, (E) high temperatures at 1C, (F) charge/discharge curves at different high temperatures, and (G) plot of open-circuit voltage at the full charge state according to bending number in the in situ bending test. GO, graphene oxide; GO-GPE, GO-modified fibrous PTC-based gel polymer electrolyte; LCO, $LiCoO_2$; PTC, poly(vinylidene fluoride-tri-fluoroethylene-chlorofluoroethylene)

separator after total 10,000 times mechanical bending. The excellent voltage stability and mechanical flexibility of GO-GPE can be attributed to the following reasons: Due to the integrated preparation process, the GO-GPE membrane develops strong adhesion with both the cathode and the anode, so, on the one hand, when the full cell is repeatedly bent, it can ensure that the active materials of the cathode and the anode will not be powdered and shed. On the other hand, the electrodes and GPE do not delaminate even if the full battery is repeatedly bent, thus significantly enhancing interface stability between the electrodes and GPE. This enhancement in strong adhesion will stabilize the electrochemical performance of flexible batteries during bending tests. In recent years, literature reports that the electrochemical performances of the flexible batteries had significantly decreased, after bending hundreds of times at most. The comparison of electrochemical and bending performances with flexible batteries reported in the literature is shown in Table S1.[47–54] To our knowledge, the flexible battery that could bend 10,000 times and cycle 1000 times was better than most of the reports.

Figure 8 shows optical images of the flexible battery connected in series with a blue light-emitting diode (LED). The battery with a charging state can light the LED continuously without change in brightness under a flat state and external bent conditions, as shown in Figure 8B,C and Video S1. More importantly, the flexible battery could still light the LED without an internal short circuit when it was cut off a corner, indicating the improved safety of the flexible battery (Figure 8D and Video S2). Recently, many commercial wearable electronic devices, such as Google Glass, smartwatch, and

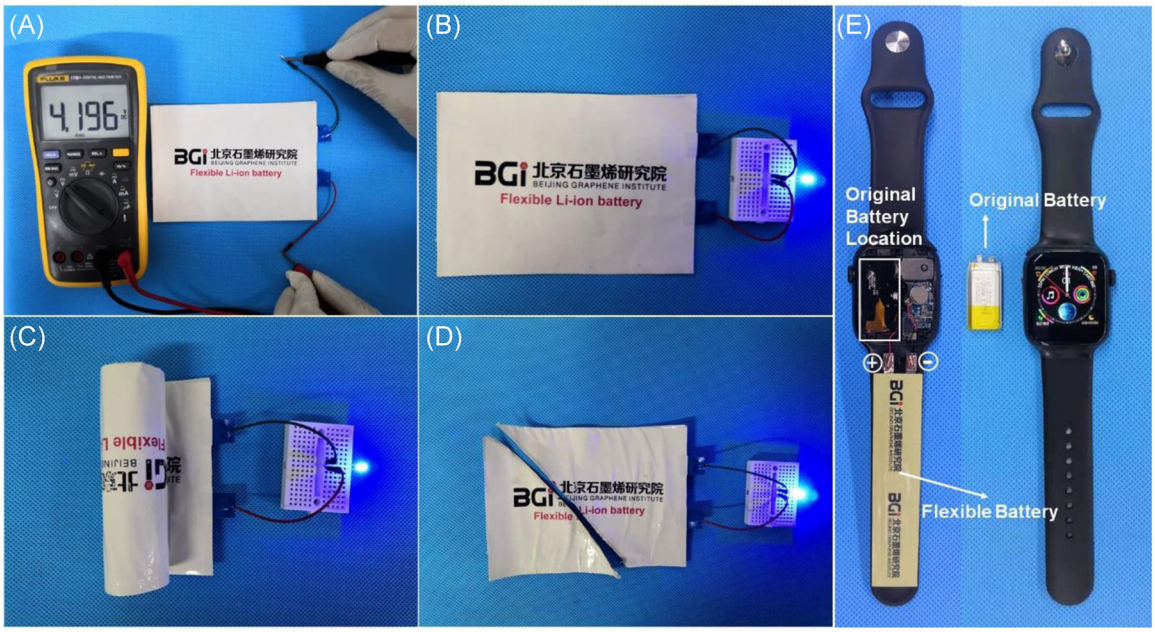

FIGURE 8 Demonstration of the flexible lithium-ion battery (LIB) connected in series with a blue light-emitting diode (LED). (A) Voltage monitoring of flexible lithium-ion battery (LIB). The battery was able to power the blue LED continuously in (B) flat, (C) bent, and (D) cropped states. (E) Demonstration of the smartwatch working properly after it was powered by the strap-like flexible LIB

smart bracelets, have been found to have limited battery life because conventional rigid LIBs with restricted sizes cannot provide sufficient capacity. This characteristic restricts the design and comfort of wearable devices. The flexible battery assembled by the GO-GPE membrane as the power source for a smartwatch is shown in Figure 8E (Video S3). Replacing the battery typically placed in the core of the smartwatch with a flexible battery that matches the shape of the watch strap results in an increased endurance of the smartwatch at least twice that of commercial products. Moreover, with the development of flexible screens, for smartwatches and bracelets, flexible LIBs are likely to be used as the power source in the future. This is powerful evidence to prove that flexible LIBs using the GO-GPE membrane have shown their unparalleled value for application in wearable devices.

4 | CONCLUSIONS

In conclusion, the present study demonstrates an extremely safe and ultrastable flexible LIB based on the integrated design of electrodes/fibrous GPEs modified with GO. It is demonstrated that such GO-GPE may not only have high ionic conductivity at a low temperature of −15°C but may also show excellent thermal stability exceeding 160°C to avoid explosion. In addition, the flexible LCO/graphite full battery using this GO-GPE shows superior electrochemical performance from −15°C to 80°C and also shows excellent cycling stability of 1000 cycles at room temperature. More importantly, the flexible LIBs using GO-GPE in this paper present excellent safety characteristics even in extremely harsh conditions, such as on being cut, bent, or even under high temperatures. Therefore, the flexible LIBs using GO-GPE have the characteristics of high-temperature resistance, nonflammability, and protection from explosion. Through integration with a smartwatch, the flexible LIBs demonstrate potential for use in intelligent wearable electronics. In conclusion, the fibrous GO-GPE and integrated design are very promising to develop next-generation gel polymer LIBs that require high flexibility, superior safety, and excellent reliability. The viability of our flexible batteries provides a potential solution to pave the way for the advancement of wearable/flexible electronics in the near future.

ACKNOWLEDGMENTS

K. Li and W. Shen contributed equally to this study. The authors also appreciate the technical assistance from the BGI Characterization & Quality Assurance Center. This study was supported by Beijing Municipal Science & Technology Commission Nos. Z181100004818004, Z181100001018029, and Z191100006119027.

CONFLICT OF INTEREST

The authors declare no conflict of interest.

ORCID

Di Wei http://orcid.org/0000-0003-2670-6362

REFERENCES

1. Wang X, Lu X, Liu B, Chen D, Tong Y, Shen G. Flexible energy-storage devices: design consideration and recent progress. *Adv Mater*. 2014;26(28):4763-4782.
2. Peng HJ, Huang JQ, Zhang Q. A review of flexible lithium–sulfur and analogous alkali metal–chalcogen rechargeable batteries. *Chem Soc Rev*. 2017;46(17):5237-5288.
3. Chen T, Qiu L, Yang Z, et al. An integrated "energy wire" for both photoelectric conversion and energy storage. *Angew Chem Int Ed*. 2012;51(48):11977-11980.
4. Shen W, Wang C, Xu Q, Liu H, Wang Y. Nitrogen-doping-induced defects of a carbon coating layer facilitate Na-storage in electrode materials. *Adv Energy Mater*. 2015;5(1):1400982.
5. Xu Y, Shen W, Wang C, Zhang A, Xu Q, Liu H. Hydrothermal synthesis and electrochemical performance of nanoparticle Li_2FeSiO_4/C cathode materials for lithium-ion batteries. *Electrochim Acta*. 2015;16:7340-7347.
6. Why is the curved screen of Samsung's Galaxy Edge really awesome. 2016. Accessed March 16, 2016. https://www.nanrenwo.net/shouji/92060.html
7. Yi L Foxconn will test the foldable iPhone from Apple. 2020. Accessed November 18, 2020. https://dy.163.com/article/FRN6PRE80544B4I1.html
8. Li YQ, Li JC, Lang XY, Wen Z, Zheng WT, Jiang Q. Lithium-ion breathable electrodes with 3D hierarchical architecture for ultrastable and high-capacity lithium storage. *Adv Funct Mater*. 2017;27(29):1700447.
9. Zhang JN, Li Q, Ouyang C, et al. Trace doping of multiple elements enables stable battery cycling of $LiCoO_2$ at 4.6 V. *Nat Energy*. 2019;4(7):594-603.
10. Cong L, Xie H, Li J. Hierarchical structures based on two-dimensional nanomaterials for rechargeable lithium batteries. *Adv Energy Mater*. 2017;7(12):1601906.
11. Wu Z, Wang Y, Liu X, et al. Carbon-nanomaterial-based flexible batteries for wearable electronics. *Adv Mater*. 2019;31(9):1800716.
12. Shen W, Li K, Lv Y, Xu T, Wei D. Liu Z. Highly-safe and ultra-stable all-flexible gel polymer lithium ion batteries aiming for scalable applications. *Adv Energy Mater*. 2020;10(21):1904281.
13. Shen W, Li H, Guo Z, et al. Double-nanocarbon synergistically modified $Na_3V_2(PO_4)_3$: an advanced cathode for high-rate and long-life sodium-ion batteries. *ACS Appl Mater Interfaces*. 2016;8(24):15341-15351.
14. Shen W, Li H, Wang C, et al. Improved electrochemical performance of the $Na_3V_2(PO_4)_3$ cathode by B-doping of the carbon coating layer for sodium-ion batteries. *J Mater Chem A*. 2015;3(29):15190-15201.
15. Yun JJ, Jeon J, Park K, Zhao X. Benefits and costs of closed innovation strategy: analysis of Samsung's Galaxy Note 7 explosion and withdrawal scandal. *J Open Innov Technol Mark Complex*. 2018;4(3):20.
16. Hovington P, Lagacé M, Guerfi A, et al. New lithium metal polymer solid state battery for an ultrahigh energy: nano C-$LiFePO_4$ versus nano $Li_{1.2}V_3O_8$. *Nano Lett*. 2015;15(4):2671-2678.
17. Theron SA, Zussman E, Yarin AL. Experimental investigation of the governing parameters in the electrospinning of polymer solutions. *Polymer*. 2004;45(6):2017-2030.
18. Raghavan P, Manuel J, Zhao X, Kim DS, Ahn JH, Nah C. Preparation and electrochemical characterization of gel polymer electrolyte based on electrospun polyacrylonitrile nonwoven membranes for lithium batteries. *J Power Sources*. 2011;196(16):6742-6749.
19. Ombaba MM, Vidu R, Jayaraman LV, Triplett M, Hsu J, Islam MS. Seamless integration of an elastomer with electrode matrix and its in-situ conversion into a solid state electrolyte for robust Li-ion batteries. *Adv Funct Mater*. 2013;23(47):5941-5951.
20. Idris NH, Rahman MM, Wang JZ, Liu HK. Microporous gel polymer electrolytes for lithium rechargeable battery application. *J Power Sources*. 2012;201:294-300.
21. Benedetti JE, Corrêa AA, Carmello M, Almeida LC, Gonçalves AS, Nogueira AF. Cross-linked gel polymer electrolyte containing multi-wall carbon nanotubes for application in dye-sensitized solar cells. *J Power Sources*. 2012;208:263-270.
22. Ryou MH, Lee YM, Cho KY, et al. A gel polymer electrolyte based on initiator-free photopolymerization for lithium secondary batteries. *Electrochim Acta*. 2012;60:23-30.
23. Sannier L, Bouchet R, Grugeon S, Naudin E, Vidal E, Tarascon JM. Room temperature lithium metal batteries based on a new gel polymer electrolyte membrane. *J Power Sources*. 2005;144(1):231-237.
24. Zhang S, Zhang N, Huang C, Ren K, Zhang QM. Microstructure and electromechanical properties of carbon nanotube/poly(vinylidene fluoride-trifluoroethylene-chlorofluoroethylene) composites. *Adv Mater*. 2005;17(15):1897-1901.
25. Liu J, Khanam Z, Ahmed S, Wang H, Wang T, Song S. A study of low-temperature solid-state supercapacitors based on Al-ion conducting polymer electrolyte and graphene electrodes. *J Power Sources*. 2021;488:229461.
26. Xu S, Sun Z, Sun C, et al. Homogeneous and fast ion conduction of PEO-based solid-state electrolyte at low temperature. *Adv Funct Mater*. 2020;30(51):2007172.
27. Du G, Tao M, Li J, et al. Low-operating temperature, high-rate and durable solid-state sodium-ion battery based on polymer electrolyte and Prussian blue cathode. *Adv Energy Mater*. 2020;10(5):1903351.
28. Lin Z, Liu J. Low-temperature all-solid-state lithium-ion batteries based on a di-cross-linked starch solid electrolyte. *RSC Adv*. 2019;9(59):34601-34606.
29. Choktaweesap N, Arayanarakul K, Aht-Ong D, Meechaisue C, Supaphol P. Electrospun gelatin fibers: effect of solvent system on morphology and fiber diameters. *Polym J*. 2007;39(6):622-631.
30. Cheng Y, Zhang L, Xu S, et al. Ionic liquid functionalized electrospun gel polymer electrolyte for use in a high-performance lithium metal battery. *J Mater Chem A*. 2018;6(38):18479-18487.
31. Yan S, Huang X, Xiao X. Measurement of the through thickness compression of a battery separator. *J Power Sources*. 2018;382:13-21.
32. Zhang F, Ma X, Cao C, Li J, Zhu Y. Poly(vinylidene fluoride)/SiO_2 composite membranes prepared by electrospinning and their excellent properties for nonwoven separators for lithium-ion batteries. *J Power Sources*. 2014;251:423-431.

33. Wicklein B, Kocjan A, Salazar-Alvarez G, et al. Thermally insulating and fire-retardant lightweight anisotropic foams based on nanocellulose and graphene oxide. *Nat Nanotechnol*. 2015;10(3):277-283.
34. Ding Y, Zhang P, Long Z, Jiang Y, Xu F, Di W. Preparation of PVdF-based electrospun membranes and their application as separators. *Sci Technol Adv Mater*. 2008;9(1):015005.
35. Raghavan P, Zhao X, Shin C, et al. Preparation and electrochemical characterization of polymer electrolytes based on electrospun poly(vinylidene fluoride-co-hexafluoropropylene)/polyacrylonitrile blend/composite membranes for lithium batteries. *J Power Sources*. 2010;195(18):6088-6094.
36. Jung HR, Lee WJ. Electrochemical characteristics of electrospun poly(methyl methacrylate)/polyvinyl chloride as gel polymer electrolytes for lithium-ion battery. *Electrochim Acta*. 2011;58:674-680.
37. Wu N, Cao Q, Wang X, Li S, Li X, Deng H. In situ ceramic fillers of electrospun thermoplastic polyurethane/poly(vinylidene fluoride) based gel polymer electrolytes for Li-ion batteries. *J Power Sources*. 2011;196(22):9751-9756.
38. Zhang Y, Yuan JJ, Song YZ, et al. Tannic acid/polyethyleneimine-decorated polypropylene separators for Li-Ion batteries and the role of the interfaces between separator and electrolyte. *Electrochim Acta*. 2018;275:25-31.
39. Yang S, Benitez R, Fuentes A, Lozano K. Dielectric analysis of VGCNF reinforced polyethylene composites. *Compos Sci Technol*. 2007;67(6):1159-1166.
40. Chiang CY, Shen YJ, Reddy MJ, Chu PP. Complexation of poly (vinylidene fluoride): LiPF6 solid polymer electrolyte with enhanced ion conduction in 'wet' form. *J Power Sources*. 2003; 123(2):222-229.
41. Xi J, Qiu X, Li J, Tang X, Zhu W, Chen L. PVDF-PEO blends based microporous polymer electrolyte: effect of PEO on pore configurations and ionic conductivity. *J Power Sources*. 2006; 157(1):501-506.
42. Cheng CL, Wan CC, Wang YY. Microporous PVdF-HFP based gel polymer electrolytes reinforced by PEGDMA network. *Electrochem Commun*. 2004;6(6):531-535.
43. Pan H, Na B, Lv R, Li C, Zhu J, Yu Z. Polar phase formation in poly(vinylidene fluoride) induced by melt annealing. *J Polym Sci B Polym Phys*. 2012;50(20):1433-1437.
44. Cai M, Yuan D, Zhang X, et al. Lithium ion battery separator with improved performance via side-by-side bicomponent electrospinning of PVDF-HFP/PI followed by 3D thermal crosslinking. *J Power Sources*. 2020;461:228123.
45. Chen YM, Hsu ST, Tseng YH, et al. Minimization of ion-solvent clusters in gel electrolytes containing graphene oxide quantum dots for lithium-ion batteries. *Small*. 2018;14(12):1703571.
46. Lin CE, Zhang H, Song YZ, Zhang Y, Yuan JJ, Zhu BK. Carboxylated polyimide separator with excellent lithium ion transport properties for a high-power density lithium-ion battery. *J Mater Chem A*. 2018;6(3):991-998.
47. Hu L, Wu H, Mantia FL, Yang Y, Cui Y. Thin, flexible secondary Li-ion paper batteries. *ACS Nano*. 2010;4(10):5843-5848.
48. Cheng Q, Song Z, Ma T, et al. Folding paper-based lithium-ion batteries for higher areal energy densities. *Nano Lett*. 2013; 13(10):4969-4974.
49. Gaikwad AM, Khau BV, Davies G, Hertzberg B, Steingart DA, Arias AC. A high areal capacity flexible lithium-ion battery with a strain-compliant design. *Adv Energy Mater*. 2015;5(3):1401389.
50. Wang Z, Wu Z, Bramnik N, Mitra S. Fabrication of high-performance flexible alkaline batteries by implementing multiwalled carbon nanotubes and copolymer separator. *Adv Mater*. 2014;26(6):970-976.
51. Chen A, Guo X, Yang S, et al. Human joint-inspired structural design for a bendable/foldable/stretchable/twistable battery: achieving multiple deformabilities. *Energy Environ Sci*. 2021; 14(6):3599-3608.
52. Xu S, Zhang Y, Cho J, et al. Stretchable batteries with self-similar serpentine interconnects and integrated wireless recharging systems. *Nat Commun*. 2013;4:1-8.
53. Park MH, Noh M, Lee S, et al. Flexible high-energy Li-ion batteries with fast-charging capability. *Nano Lett*. 2014;14(7): 4083-4089.
54. Wang XF, Lu XH, Liu B, et al. Flexible energy-storage devices: design consideration and recent progress. *Adv Mater*. 2014; 26(28):4763-4782.
55. Choi Y, Zhang K, Chung KY, Wang DH, Park JH. PVdF-HFP/exfoliated graphene oxide nanosheet hybrid separators for thermally stable Li-ion batteries. *RSC Adv*. 2016;6(84): 80706-80711.
56. Kashiwagi T, Du F, Douglas JF, Winey KI, Harris RH, Shields JR. Nanoparticle networks reduce the flammability of polymer nanocomposites. *Nat Mater*. 2005;4(12):928-933.

SUPPORTING INFORMATION

Additional Supporting Information may be found online in the supporting information tab for this article.

How to cite this article: Li K, Shen W, Xu T, et al. Fibrous gel polymer electrolyte for an ultrastable and highly safe flexible lithium-ion battery in a wide temperature range. *Carbon Energy*. 2021;3:916-928.
https://doi.org/10.1002/cey2.151